Available online at www.sciencedirect.com

jmr&t Journal of Materials Research and Technology

journal homepage: www.elsevier.com/locate/jmrt

Original Article

Solid coin-like design activated carbon nanospheres derived from shallot peel precursor for boosting supercapacitor performance

Erman Taer [a,*], *Apriwandi Apriwandi* [a], *Dhea Rama Andani* [a], *Rika Taslim* [b,**]

[a] *Department of Physics, Faculty of Mathematic and Natural Sciences, University of Riau, Simpang Baru, Riau, 28293, Indonesia*

[b] *Department of Industrial Engineering, State Islamic University of Sultan Syarif Kasim, Simpang Baru, Riau, 28293, Indonesia*

ARTICLE INFO

Article history:
Received 8 August 2021
Accepted 6 September 2021
Available online 14 September 2021

Keywords:
Nanosphere
Nanofiber
Nanosheet
Electrode material
Supercapacitor

ABSTRACT

Thin porous carbon nanospheres based on natural materials, characterized by abundant availability, facile synthesis without templates, and heteroatom doping have confirmed the enhanced high performance of electrochemical energy storage devices. However, these potentials are difficult to obtain, and further poses a serious challenge. This work, activated carbon nanosphere was obtained from the biomass precursor shallot peel through a solid coin-like design with different chemical impregnations with high-temperature pyrolysis. The three different activators used were KOH, $ZnCl_2$, and NaOH, selected to optimize the precursor's potential to produce porous carbon nanospheres. All the carbons prepared exhibited potential nano-sized morphological structures with a high carbon content of 77.71–90.11%. Furthermore, the oxygen content of 24.60% indicated a doping heteroatom for the electrode material. Surprisingly, the KOH impregnation exhibited a nanosphere-rich morphological structure with a diameter of 102–124 nm adhering to the nanofiber surface. This combination of material properties has the benefit of improving the supercapacitor's performance with a high specific capacitance of 170.12 F g^{-1} in a 1 M H_2SO_4 aqueous electrolyte. Meanwhile, the maximum specific energy reached 16.67 Wh kg^{-1} with a maximum specific power of 86.40 W kg^{-1} at a constant current density of 1.0 A g^{-1}, in a two-electrode system. Therefore, the activated carbon with a solid coin-like design derived from shallot peel waste is a potential source of a rich nanospheres structure with a facile strategy for large-scale commercial electrochemical energy storage applications.

* Corresponding author.
** Corresponding author.
E-mail addresses: erman.taer@lecturer.unri.ac.id (E. Taer), rikataslim@gmail.com (R. Taslim).

https://doi.org/10.1016/j.jmrt.2021.09.025

1. Introduction

Rapid industrial and technological development plays an important role in changing the global community's social life. This has led to a significant increase in the use of high-end smartphones, tablets, laptops, personal computers, as well as high-quality cameras, and consequently, triggers high energy consumption, as well as environmental damage. Recently, researchers have focused on the procurement of environmentally friendly electrical technology and optimization of storage devices for electrical energy, particularly batteries, supercapacitors, and electrolytic capacitors. The hybrid electric vehicle model has been considered as one of the latest technological evolutionary progress initiating the intense study of energy storage devices with enhanced electrodes, especially lithium-ion batteries and high-performance supercapacitors [1,2]. In addition, supercapacitors are high-performance electrochemical storage devices with cheaper, as well as more effective, and efficient electrode materials, compared to lithium-ion batteries [3]. These devices also have considerably infinite cycle life, high power density, excellent reversibility, and higher power density, and therefore, show promising application in various sectors, especially in electric vehicle systems [4,5]. The consumption of fuel oil and natural gas for industrial vehicles and machinery leads to environmental pollution, followed by the depletion of these non-renewable resources, and also shows the need to develop high-performance supercapacitors based on inexpensive, easily synthesized, as well as highly effective electrode materials. Numerous raw materials have been studied to obtain superior electrodes for supercapacitors, including polymers [6,7], graphene oxide [8], metal oxides [9–11], carbon black [12], and biomass-based porous carbon [13,14]. However, biomass-based carbon is cheap, easy to obtain, abundantly available, as well as pollution-free, and is, therefore, more popular, compared to the other materials [15]. Furthermore, this is a suitable alternative solution to reduce toxic waste from the by-products of industrial activities [16,17]. Recently, agricultural by-products have shown outstanding supercapacitor performance, obtaining surface areas of up to >2000 m^2g^{-1}, and this is able to improve the specific capacitance properties by about 400 Fg^{-1} [18–20]. Most importantly, the specific energy is increasable by up to 3 times, compared to the review studies by optimizing pore characteristics by hierarchically interconnecting 3D pores between micro, meso, and macropores [20,21]. This is the answer to the main challenge of supercapacitor-related studies where the specific energy was reported to be lower, compared to the specific power. However, not all biomass is able to produce a 3D hierarchical pore structure including micro, meso, and macropores. Also, the material's benefits are limited by the relatively complex preparation methods using templates, metal frameworks, and the addition of synthetic materials. Researchers believe this challenge is bound to be overcome by changing the particle size and up to nano size. Furthermore, carbon nanospheres have shown high specific surface area advantages, providing well-connected diverse pore structures, high conductivity, as well as good chemical-thermal stability, and this is able to promote high specific energies in electrochemical energy storage devices [22,23]. Zheng et al., (2021) reported the superiority of the nanosphere's structure has the capacity to increase the specific energy to 71.9 $Whkg^{-1}$, with a specific capacitance of 273.9 Fg^{-1} [24]. Zhou et al., (2021) also reported a similar finding, with an ultra-high specific capacitance of 1214 Fg^{-1} [25]. However, these studies mostly used polymeric materials as well as metal oxides for fabrication, and the method presented is relatively complex, requires various instruments, and has toxic side effects. Recently, He et al., (2021) studied the potential of red rod biomass waste in producing hierarchically porous hollow carbon nanospheres through a one-step by thermal treatment, and reported a surface area of 1792 m^2g^{-1}, with a specific capacitance of 198.6 Fg^{-1} [26]. In addition, the method reported is relatively simple, and reproducible with standard instruments. This confirms natural materials are a potential source of nanosphere structures, although this is not confirmed in all biomass.

In this study, porous carbon nanospheres were produced from shallot peel agricultural waste through a simple and feasible strategy with chemical impregnation of KOH, $ZnCl_2$, and NaOH at high-temperature pyrolysis. Several chemical activations were applied to optimize the precursor's potential morphological structure. The porous carbon was prepared in the form of an adhesive-free solid with a coin-like design as a basic approximation to maintain the real conductivity properties, and the porous carbon obtained possessed a nanosphere structure followed by nanofibers and nanosheets with a specific surface area of 1182.3 m^2g^{-1}. Most importantly, the KOH impregnation produced a nanosphere-rich morphological structure with a diameter of 102–124 nm adhering to the nanofiber surface. The supercapacitor cell system's high electrochemical properties were confirmed with a specific capacitance of 170 Fg^{-1} at a current density of 1.0 Ag^{-1}, through a two-electrode configuration. Meanwhile, the maximum specific energy was discovered to reach 16.67 Wh kg^{-1}, with a maximum specific power of 86.40 Wkg^{-1} in 1 M H_2SO_4 aqueous electrolyte. Therefore, environmentally friendly, inexpensive, and controlled carbon nanospheres were obtained from shallot peel biomass precursors as electrode material for high-performance electrochemical energy storage devices, using a chemical impregnation method at high-temperature pyrolysis.

2. Materials and methods

2.1. Materials

The selected biomass raw material was shallot peels waste obtained from vegetable farmers in Pekanbaru city. Subsequently, the samples were dried in two stages: under direct sunlight and in an oven vacuum at 110 °C. This was followed by crushing and grinding the dried shallot peels into powder with particle size <60 μm. Meanwhile, the chemical activating agents used, KOH, $ZnCl_2$, and NaOH in a 0.5 mL^{-1} solution, were purchased from several brands including Sigma Aldrich and Merck KGaA, respectively. In the electrochemical analysis, the electrolyte prepared was a 1M H_2SO_4 solution obtained from Panreac Quimica Sau while the separator was

selected from the organic material of the duck eggshell cell membrane.

2.2. Synthesis of shallot peel-based nanospheres activated carbon

For this experiment, 30g of Shallot peel (SP) powder were chemically impregnated separately, using KOH, $ZnCl_2$, and NaOH solutions, then oven-dried at 110°C for 36–48 h. The chemically impregnated carbon powder was then converted to a solid coin-like shape by passing through a hydraulic press instrument under a pressure equivalent to a load of ±8ton. This solid coin-like design was prepared without the addition of adhesives, by purely optimizing the raw material's self-adhesive. A total of 15 solid coin-like carbon were then placed into the furnace tube for high-temperature pyrolysis involving carbonization and physical activation processes in the N_2 and CO_2 gas environments. The optimum temperatures for carbonization and physical activation are 600°C with a temperature increase of 3 °C/min and 900°C with a temperature increase of 10 °C/min, respectively. Subsequently, all samples were neutralized by immersion in DI water.

2.3. Material characterization

The density of samples designed to possess a solid coin-like shape without the use of adhesive materials must be evaluated through measurements of mass, diameter, and thickness. In this study, the microcrystalline phase change behavior was analyzed by X-ray diffraction (Shimadzu-XRF-7000L) at a 2θ angle range of 10–60° with CuKα as the irradiation source, while the microcrystalline dimensions were evaluated using the debye-Scheerer equation [27]. Furthermore, the material's morphology and surface structure were analyzed using the scanning electron microscopy method at a maximum voltage of 15Kv (JSM-6510A/JSM-6510LA), while the elemental composition was confirmed using energy dispersive spectroscopy in the energy range of 0–20 keV (JSM-6510A/JSM-6510LA).

2.4. Confirmation of electrochemical properties

The electrochemical properties of nanospheres activated carbon based on shallot peel waste were evaluated through the general cyclic voltammetry (CV) and galvanostatic charge–discharge (GCD) technique. Furthermore, the supercapacitor cell was prepared in a two-electrode configuration comprising two solid coin-like activated carbons designed without adhesive and separated by an organic separator in an aqueous electrolyte solution of 1M H_2SO_4, with a working mass of ±0.0101g. The cyclic voltammetry method was performed at a maximum potential window of 0–1V in several scan rates including 1,2, 5, and 10 mV s^{-1}, and the specific capacitance was evaluated using the standard equation [28,29]. Also, the galvanostatic charge discharge was evaluated at a constant current density of 1.0 A g^{-1}, while the specific capacitance, specific energy, and specific power were determined using standard equations [30].

3. Results and discussions

3.1. Materials properties analysis

Density change is an initial analysis performed to evaluate the material properties of the activated carbon designed to resemble a solid coin without any adhesive material. The chemical impregnation processes using KOH, $ZnCl_2$, and NaOH treatments at high-temperature pyrolysis directly affect the coin's density through reduced mass, thickness, and diameter. The high-temperature pyrolysis and a certain temperature rise led to evaporation of the water content, volatile elements, and other light compounds [31]. Generally, Shallot peel as raw material contains hemicellulose, cellulose, as well as lignin compounds incorporated in the lignocellulosic components, and this undergoes decomposition, as well as reduction at different temperatures. Furthermore, the carbonization process in an N_2 gas environment at a maximum chamber temperature of 600°C is able to produce carbon fixed from precursor samples through evaporation of the water content and reduction of the lignocellulosic components, consequently, reducing the sample's density [32]. However, the residual content of tar as a by-product of carbonization is considered to hinder optimized carbon pores framework expansions, therefore, further physical activation processes are required in a CO_2 gas environment [33]. According to Fig. 1, the physical activation process was performed at 600°C–900°C to reduce as well as degrade cellulose and lignin compounds, maximizes pore expansion, while opening narrow pores on the activated carbon surface, consequently, reducing the activated carbon's density [34]. The three shallot peel-based activated carbon samples experienced a reduction in density after a high-temperature pyrolysis process, including carbonization and physical activation integrated into one step. Before the pyrolysis, the densities of activated carbon of the SP-KOH, SP-$ZnCl_2$, and SP-NaOH samples were 0.8890, 1.0946, as well as 0.8075 g cm^{-3}, respectively, and after the pyrolysis, the densities were 0.8455, 0.8489, and 0.5889 g cm^{-3}, respectively. The largest density

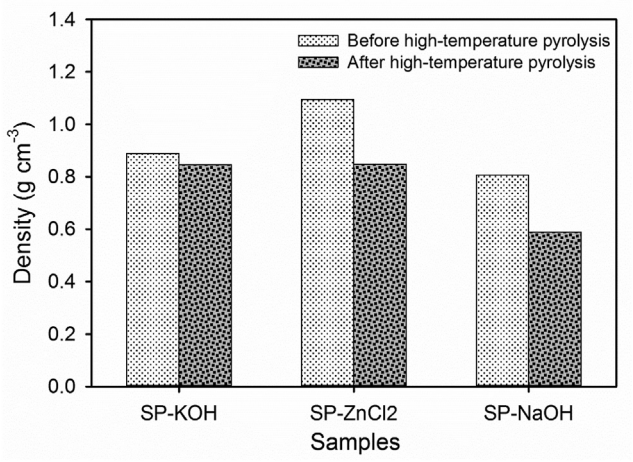

Fig. 1 – Change in density of coinlike porous carbon nanosphere.

reduction of 27.07% was obtained in the SP-NaOH sample, followed by the SP-$ZnCl_2$ and SP-KOH samples at 22.44% and 4.89%, respectively. Therefore, chemical activation also significantly affects the sample's density, due to the activating reagents' features and reactions with carbon at different temperatures. This study's density analysis is in agreement with previously reported studies using different precursors, including reed waste [35], and durian shell [36].

Fig. 2 shows the X-ray diffraction analysis on the microcrystalline phases of the three activated carbons obtained. The XRD pattern for the SP-KOH, SP-$ZnCl_2$, and SP-NaOH samples was evaluated at an angle range of 10°–60°. Generally, all samples showed two broad peaks at $2\theta = 24°$ and 45°, followed by several sharp peaks at different angles. The broad peaks at $2\theta = 24°$ and 45° correlated with the scattering planes 002 and 100, confirming the turbostratic disturbed carbon structure and leading to desirable amorphous properties [37]. This property helps the electrode material to provide an ionic charge contact area in optimizing the supercapacitor's high performance. In addition, the SP-KOH sample displayed two larger broad peaks, compared to the SP-$ZnCl_2$ and SP-NaOH samples, especially in the 002 reflection plane. This is probably due to the carbon surface's increasingly irregular structure, initiating the formation of various pore sizes [38]. This is in agreement with several case studies, where similar cases were also reported [39]. Also, sharp peaks were found at different angles, including 28.1–29.4°, 33.1°, 37.6°, 45.8–46.3°, and 48.8°, confirming the presence of crystalline compounds in almost all samples, particularly CaO/$CaCO_3$, MgO, and SiO_2 compounds. Cao/$CaCO_3$ compounds were found at 28.1–29.4°, and 48.8° (JCPDS No. 82-1690), while MgO compounds were confirmed at 45.8–46.3°, and SiO_2 compounds at 33.1° and 37.6° (JCPDS No. 89-1668). The presence of these compounds is partially due to basic constituents of the biomass precursors subjected to oxidative stress during pyrolysis. These results were also confirmed through elemental analysis using EDS.

Table 1 provides a detailed summary of the interlayer spacing d_{002}-d_{100} and microcrystalline dimensions L_c-L_a for chemically impregnated activated carbon. The d_{002} and d_{001} values of SP-KOH, SP-$ZnCl_2$, and SP-NaOH are reasonable for bio-waste-based amorphous carbon. Furthermore, d_{002} has a relatively higher value of 9.09%, compared to d_{002} for normal graphite, confirming the irregular (turbostratic) carbon structure. Meanwhile, the microcrystalline dimensions, especially L_c, are closely related to the prediction of the specific surface area of carbonaceous materials through empirical equations $SSA_{XRD} = 2/\rho_{XRD}L_c$, as previously reported [40,41]. L_c is a parameter inversely proportional to the specific surface area, therefore, a low L_c implies a high surface area. The least L_c value was obtained in the SP-KOH sample, indicating the specific surface area was predicted to reach 1182.23 $m^2\ g^{-1}$, while the SP-$ZnCl_2$ and SP-NaOH counterparts were 1058.58 $m^2\ g^{-1}$ and 597.78 $m^2\ g^{-1}$, respectively. Table 1 presents the detailed summary of the SSA_{XRD} properties for the three samples. These properties are required to improve the electrode material's electrochemical properties for electrochemical energy storage applications.

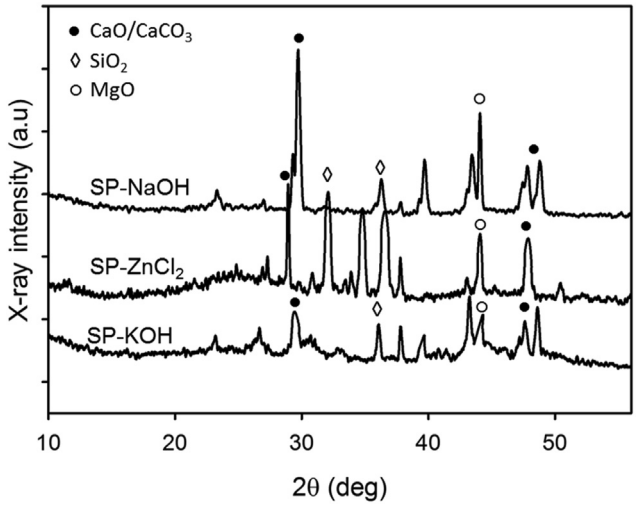

Fig. 2 – XRD pattern of coinlike porous carbon nanosphere.

The coin-like activated carbon's morphological structure was evaluated using scanning electron microscopy. Fig. 3 shows the SEM image for the chemically impregnated green shallot-based activated carbon samples of KOH, $ZnCl_2$, and NaOH. According to the diagram, the samples retained the basic structure of the biomass-based precursors, and exhibited the morphology as well as structure of nanospheres and nanofibers, with relatively varied sizes, mainly due to the difference in the activating chemical agents. In the carbonization and high-temperature activation processes, the chemical reagent dehydrates and degrades the complex lignocellulosic compounds with the ability to reveal unique structures and morphology on the sample [42]. The Lignin component contributes to the appearance of tubular structures and is speculated to present nanospheres on porous carbon-based biomass [42]. Meanwhile, the cellulose degraded due to high temperature contributes to the nanofiber structure [43]. Fig. 3a shows the KOH impregnated samples displayed a distinct surface morphology rich in nanospheres dotted with nanofibers. The nanosphere's diameter ranges from 102 nm to 124 nm, while the fiber diameter ranges from 135 to 370 nm. In the selected magnification area, the nanospheres are seen to adhere to almost all the fiber surfaces, and are closely interrelated, initiating hierarchically connected pore channels while minimizing agglomeration, and consequently, ensuring more effective ion contact sites and charge transport pathways for electrochemical energy storage [24]. Fig. 3b shows the $ZnCl_2$ impregnated sample, confirming the rod-like morphological structure with a diameter of 362–882 nm and a predominant clump of carbon blocks. The nanofibers with a diameter of 168–196 nm were also confirmed to be clear in relatively small amounts, compared to the SP-KOH samples, while the nanospheres with a diameter of 161–128 nm, were confirmed to adhere to the fiber's surfaces, although in relatively small amounts. In addition, the activation of $ZnCl_2$ is speculated to be able to reduce the structure of nanospheres and nanofibers. At pyrolysis temperatures of >500 °C, $ZnCl_2$ reacts with the carbon matrix framework to produce oxidative compounds [44]. Numerous functional groups containing oxygen in the nano-spherical structure are evaporated by $ZnCl_2$ in the form of H_2O and CO, consequently, reducing the number of nanospheres on the sample's surface morphology [45]. Furthermore, the byproduct of the chemical reaction in the

Table 1 – The interlayer spacing, dimension microcrystalline and specific surface area of coinlike porous carbon nanosphere.

Samples	$2\theta_{002}$ (°)	$2\theta_{100}$ (°)	d_{002} (Å)	d_{100} (Å)	L_c (Å)	L_a (Å)	SSA_{XRD}
SP-KOH	25.453	44.260	3.596	2.044	8.042	49.177	1182.23
SP-$ZnCl_2$	24.241	43.499	3.668	2.078	9.161	16.707	1058.58
SP-NaOH	23.431	42.037	3.499	2.147	15.482	39.858	597.78

form of ZnO simultaneously erodes the carbon sphere, producing mostly micropores in the nano-spherical structure. However, this is able to simultaneously cause the collapse of large carbon nanospheres to form carbon blocks, and causes a smaller diameter in the nanofiber structure, compared to the SP-KOH sample. This structure has the capacity to increase the electrode material's conductivity and improve the supercapacitor's capacitive properties [46].

Fig. 3c shows the SP-NaOH sample's morphology with relatively confirmed short nanofiber structures of 78–250 nm diameter, as well as a unique flower-like structure. In the selected magnification area, the SP-NaOH sample exhibits a sheet structure with a thickness of 26–56 nm. The NaOH reaction at high-temperature pyrolysis is able to maintain the basic structure of the cellulose precursor, Na_2CO_3 as the reaction's first product, to initiate the formation of oxidative compounds NaO_2 by evaporating CO and H_2O compounds [47]. This is able to decompose the lignocellulosic material's carbon framework and maintain the structure of the fibers and sheets in the sample [48]. Also, this combination of structures has greatly contributed to discovering the ideal material for high-performance supercapacitor electrodes [49].

Table 2 presents a detailed summary of the elemental status of shallot peel-based activated carbon with different chemical impregnations. Generally, the three samples confirmed carbon had the highest elemental percentage of about 77.71%–90.11%. This showed chemical impregnation at high-temperature pyrolysis in N_2 and CO_2 environments

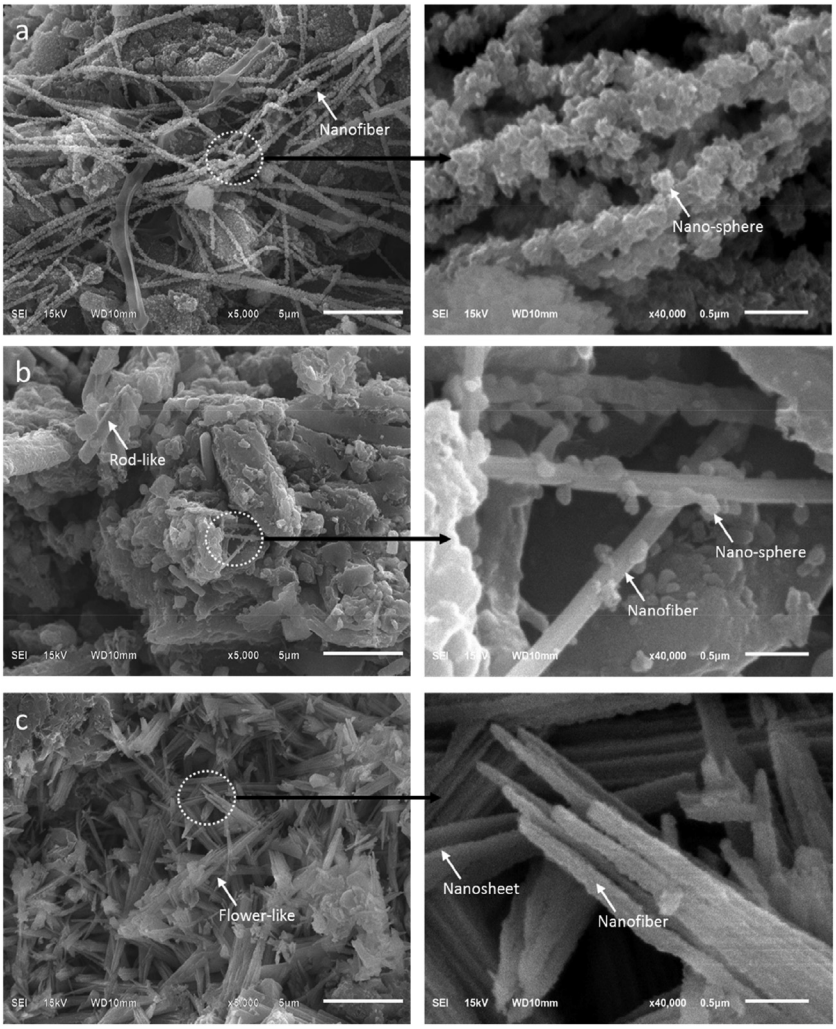

Fig. 3 – SEM image of (a) SP-KOH, (b) SP-$ZnCl_2$, dan (c) SP-NaOH.

Table 2 – Elemental analysis of coinlike porous carbon nanosphere.

Samples	Element analysis					
	C (%)	O (%)	Mg (%)	Ca (%)	Si (%)	K (%)
SP-KOH	77.71	18.60	1.04	1.91	0.51	0.23
SP-$ZnCl_2$	69.18	24.74	0.91	4.83	0.29	0.05
SP-NaOH	90.11	8.57	0.41	0.62	0.26	0.03

successfully converted biomass precursors into high purity carbon. The SP-NaOH sample produced the highest carbon of 90.11% followed by the SP-KOH sample, and SP-$ZnCl_2$ 77.71% and 69.11%, respectively. Therefore, the provision of electron and ion charge active surface sites to form a high electrochemical double-layer is highly beneficial. Meanwhile, oxygen had the second-highest elemental percentages ranging from 18.60% to 24.74%. This indicates the presence of oxidative compounds, for instance, CaO/$CaCO_3$, MgO, and SiO_2 in all samples. These results are confirmed to be the same as the previously discussed XRD pattern analysis. This elemental oxygen tends to provide wettability properties for ions to diffuse at the electrode/electrolyte interface [50]. Also, other contaminants including Mg, Ca, Si, and K are present in oxidative compounds in relatively minute amounts, due to the basic biomass components partially decomposed during the high-temperature pyrolysis process [51].

3.2. *Electrochemical behavior analysis*

The electrochemical properties of supercapacitor cells were confirmed through cyclic voltammetry and galvanostatic charge–discharge techniques in a two-electrode configuration system. Supercapacitor cells were prepared in the form of a sandwich layer with activated carbon in a coin-like design, without the addition of adhesives, including PVP or PFDV. The electrolyte selected was aqueous electrolyte 1M H_2SO_4, while the organic separator used was derived from duck eggshell membrane. Fig. 4 shows the cyclic voltammetry profiles for all three samples evaluated at a scan rate of 1 mVs^{-1}. The image shows a distorted rectangular shape indicating the relatively ideal electrochemical double-layer properties of porous carbon-based biomass [52]. Furthermore, the high oxygen content of 24.70% contributed to the sample's wettability, and this possibly exerted a pseudocapacitance effect on the sample [53]. This profile has not been completely confirmed, however, this is faintly visible in the SP-KOH sample, where a slight surge current density in the voltage range of 0.2–0.6V occurred. The area sweep of the closed hysteresis loop also confirmed the electrode material's capacitive behavior, where the largest hysteresis loop was found in the SP-KOH samples and exhibited the highest capacitive property, followed by SP-$ZnCl_2$ and SP-NaOH. Based on standard equation, the SP-KOH, SP-$ZnCl_2$, and SP-NaOH samples had specific capacitances of 151, 116, and 91 Fg^{-1}, respectively.

The thin diameter nano-spherical structure allows the carbon matrix framework to exhibit a high specific surface area of 1182.23 m^2g^{-1} and a variety of pore structures in the <50 nm size range, therefore, enabling rich micropores and mesopores in activated carbon [24]. The high surface area

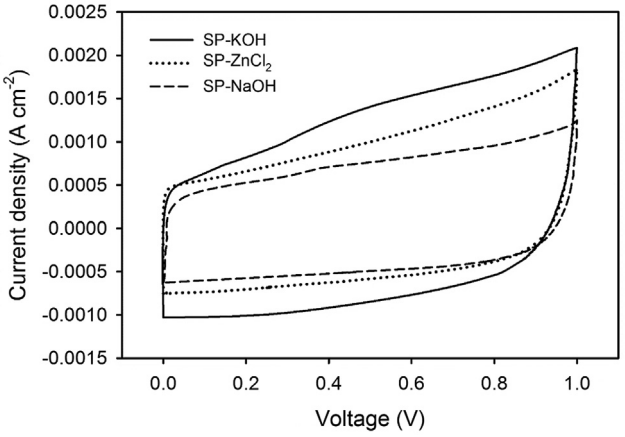

Fig. 4 – CV voltammogram of SP-KOH, SP-$ZnCl_2$, and SP-NaOH at scan rate of 1 mV s^{-1}.

initiated by the micropores structure contributes to the provision of an active site for the charge diffusion of the electrolyte ions on the electrode surface [20]. In addition, the mesopores confirm the larger charge-carrying channel and consequently, low internal resistance. This combination significantly increases the electrode material's specific capacitance as shown in the SP-KOH sample, while the nanofibers structure is responsible for the high conductivity [54]. The electrodes' performances were also evaluated through differences in scanning rates. Fig. 5a–c shows the SP-KOH, SP-$ZnCl_2$, and SP-NaOH samples displayed CV curves at scan rates of 1, 2, and 5 mV s^{-1}. The CV profile also forms a distorted rectangular curve indicating normal EDLC behavior, and a quicker saturation rate. The application of the scanning rate also significantly affects the carbon electrode's capacitive properties. According to Fig. 5d, the specific capacitance is reduced at lower scan rates to 10 mVs^{-1}, confirming the uncontrolled pore structure hindering the transport of electrolyte ions on the electrode surface. SP-$ZnCl_2$ does not possess the highest capacitive properties as well as specific surface area, however, the sample is able to maintain the highest specific capacitance of about 67.4% at a high scanning rate of 10 mVs^{-1}. This is due to the presence of a nanofiber structure contributing to increased conductivity, and consequently maintain the electrochemical properties [54].

Fig. 6 shows all samples exhibited a perturbed isosceles triangular GCD profile at a constant current density of 1.0 Ag^{-1}, confirming the normal double-layer electrochemical properties, and this is consistent with the CV curve shown in Fig. 4. Also, the iR drop was found to be insignificantly indicative of relatively low resistance in the electrode material. The charging and discharging times in the GCD profile significantly confirm the supercapacitor cell's performance, with the longest discharge time obtained in SP-KOH samples, indicating the highest capacitive properties, followed by SP-$ZnCl_2$ and SP-NaOH samples. Based on standard forlmula, the specific capacitances obtained for SP-KOH, SP-$ZnCl_2$, and SP-NaOH samples are 170.12, 127.4, as well as 79.2 Fg^{-1}, respectively, and these values correspond to the data obtained from the CV technique.

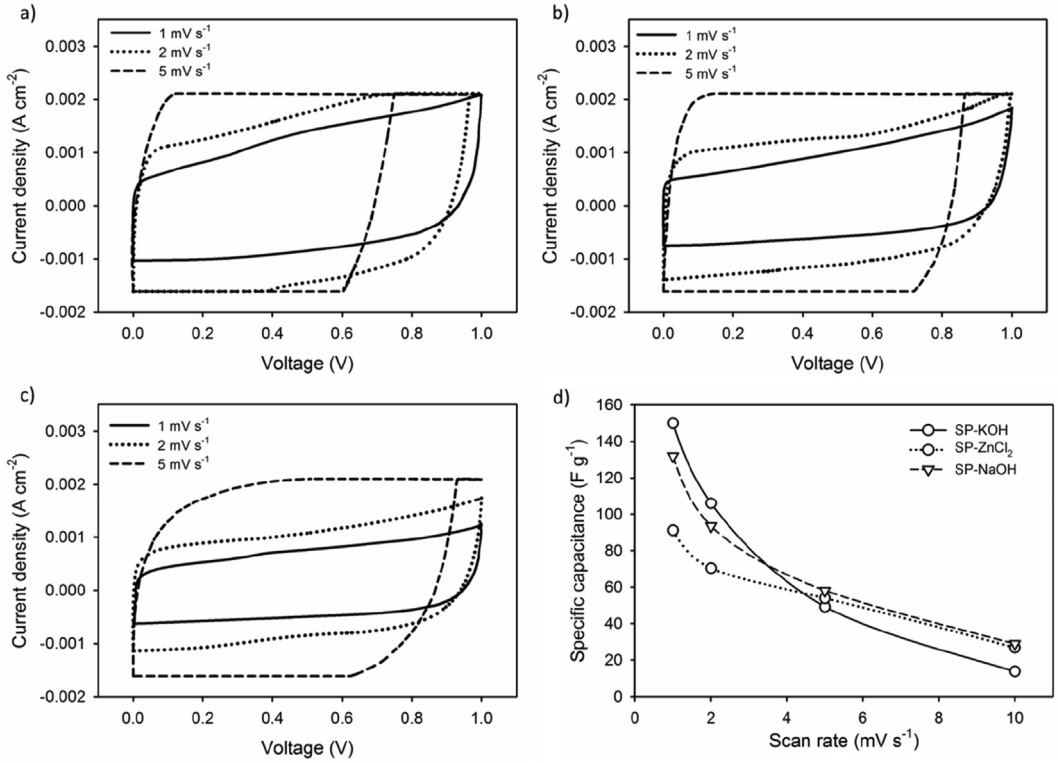

Fig. 5 – CV voltammogram at different scan rate of (a) SP-KOH, (b) SP-ZnCl2, (c) SP-NaOH, and (d) specific capacitance vs. scan rate.

In addition, SP-KOH has superior material properties compared to the other two samples, especially the morphology and structure of thin nanospheres followed by nanofibers with higher specific surface area. This combination of nano-sized structures allows the formation of diverse pores, therefore, imparting high microporosity as well as mesoporosity properties in the sample, and this leads to a high surface area and larger ion diffusion pathway, consequently, improving the supercapacitor's performance [55]. In this study, the presence of thin diameter nanospheres in SP-KOH samples resulted in the relatively higher internal resistance of 31 mΩ, compared to the SP-$ZnCl_2$ and SP-NaOH counterparts of 22 mΩ and 10 mΩ, respectively. The presence of thin diameter nanospheres allows a more dominant distribution of small pores and provides more electron/ion active sites at the electrolyte/electrode interface [23,26]. However, this in turn often significantly narrows the ionic charges' migration path, consequently, increasing the internal resistance. In contrast to the SP-NaOH samples, the presence of a nanosheet structure is able to shorten the ions' migration path significantly, therefore, enabling free diffusion without interference at the electrolyte/electrode interface, while

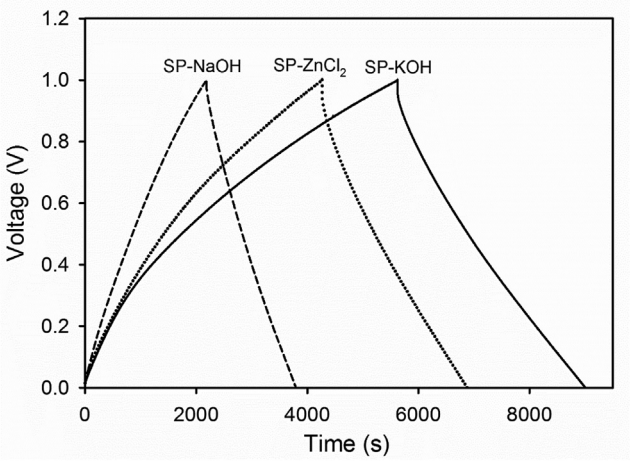

Fig. 6 – GCD profile of SP-KOH, SP-$ZnCl_2$, and SP-NaOH at current density of 1.0 A g^{-1}.

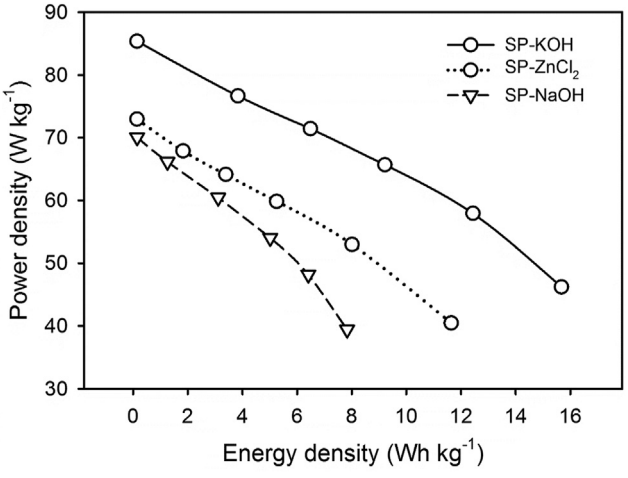

Fig. 7 – Ragone plot of energy specific and power density of coinlike porous carbon nanosphere.

Table 3 – Comparison of electrochemical properties of various sources of electrode materials.

Sources	Structures	SSA ($m^2\ g^{-1}$)	Electrode type	C_{sp} ($F\ g^{-1}$)	Electrolyte	E ($Wh\ kg^{-1}$)	P ($W\ kg^{-1}$)	R (Ω)	refs
Reed rod	Nanosphere	1792	powder	198.6	6 M KOH	3.5	20k	0.29	[26]
Glucose	Nanosphere	1210	Powder	282	6 M KOH	8.5	250	1.04	[22]
Pyrrole-based	Nanosphere	1347	Powder	395	6 M KOH	–	–	0.77	[23]
Nickel and Cobalt MOF-derived	Microsphere	1135	Powder	1214	2 M KOH	55.4	758.5	0.93	[25]
Quinone-amine polymer	Nanosphere	2671.2	Powder	273.9	6 M KOH	8.0	80.3	–	[24]
American poplar fruit	Tubular-like	942	Coin-type	58.71	6 M KOH	7.99	372	1.97	[56]
Cassava petiole	Rod-like	759.81	Monolith	193.68	1 M H_2SO_4	26.90	96.94	–	[39]
Shallot peel	Nanosphere	1182.2	Coinlike	170.12	1 M H_2SO_4	16.67	86.40	0.031	This work

producing the least internal resistance, as reported in previous studies [49].

The specific energy and specific power of the shallot peel-based activated carbon were evaluated using standard equations (Fig. 7). The Ragone plot shows the highest specific energy of 16.67 $Whkg^{-1}$ found in the SP-KOH sample with a maximum specific power of 86.40 Wkg^{-1} at a constant current density of 1.0 Ag^{-1}, followed by SP-$ZnCl_2$ and SP-NaOH samples with specific energies of 12.64 and 8.82 $Whkg^{-1}$ at the maximum specific power of 73.96 and 71.07 Wkg^{-1}, respectively. According to Table 3, the maximum specific energy obtained in this study is considerably greater, compared to other reports where relatively complex methods requiring synthetic base materials were used.

4. Conclusion

Biomass waste of shallot peel-based activated carbon nanospheres was successfully prepared using a solid coin-like design and impregnation with different chemicals at high-temperature pyrolysis. Furthermore, three chemical activating agents were selected to maximize the precursors' potential to produce nano-sized structures. All samples were confirmed to possess relatively adequate amorphous properties for biomass-based porous carbon. Each activator significantly produces different nanostructures including nanospheres, followed by nanofibers and nanosheets. SP-KOH exhibits a morphological structure rich in thin nanospheres adhering tightly to the nanofiber surface, while SP-$ZnCl_2$ consistently displays nanofiber morphology with reduced nanospheres. Interestingly, SP-NaOH provides a favorable nanosheet structure to reduce the electrode material's resistance. The combination of these nanostructural properties is able to increase the material's specific capacitance by 170.12 $F\ g^{-1}$ in the 1 M H_2SO_4 electrolyte. These results confirm the solid coin-like design of the activated carbon of the onion peel is a remarkable innovation to obtain high-performance electrode materials for energy storage applications.

Declaration of Competing Interest

The authors declare that they have no known competing financial interests or personal relationships that could have appeared to influence the work reported in this paper.

Acknowledgement

The work was financially supported by Kementerian Pendidikan, Kebudayaan, Riset, dan Teknologi, Repulic of Indonesia through first year Project of world Class Research (WCR) contract No. 1393/UN.19.5.1.3/PT.01.03/2021.

REFERENCES

[1] Sharma P, Bhatti TS. A review on electrochemical double-layer capacitors. Energy Convers Manag 2010;51:2901–12. https://doi.org/10.1016/j.enconman.2010.06.031.
[2] Chen T, Dai L. Carbon nanomaterials for high-performance supercapacitors. Mater Today 2013;16:272–80. https://doi.org/10.1016/j.mattod.2013.07.002.
[3] Mensah-Darkwa K, Zequine C, Kahol PK, Gupta RK. Supercapacitor energy storage device using biowastes: a sustainable approach to green energy. Sustain 2019;11. https://doi.org/10.3390/su11020414.
[4] Poonam Sharma K, Arora A, Tripathi SK. Review of supercapacitors: materials and devices. J Energy Storage 2019;21:801–25. https://doi.org/10.1016/j.est.2019.01.010.
[5] González A, Goikolea E, Barrena JA, Mysyk R. Review on supercapacitors: technologies and materials. Renew Sustain Energy Rev 2016;58:1189–206. https://doi.org/10.1016/j.rser.2015.12.249.
[6] Wu ZY, Liang HW, Chen LF, Hu BC, Yu SH. Bacterial cellulose: a robust platform for design of three dimensional carbon-based functional nanomaterials. Acc Chem Res 2016;49:96–105. https://doi.org/10.1021/acs.accounts.5b00380.
[7] Miller EE, Hua Y, Tezel FH. Materials for energy storage: review of electrode materials and methods of increasing capacitance for supercapacitors. J Energy Storage 2018;20:30–40. https://doi.org/10.1016/j.est.2018.08.009.
[8] Shen W, Zang J, Hu H, Xu J, Zhang Z, Yan R, et al. Controlled synthesis of KCu7S4/rGO nanocomposites for electrochemical energy storage. Mater Des 2020;195:108992. https://doi.org/10.1016/j.matdes.2020.108992.
[9] Bai Y, Liu R, Li E, Li X, Liu Y, Yuan G. Graphene/Carbon Nanotube/Bacterial Cellulose assisted supporting for polypyrrole towards flexible supercapacitor applications. J Alloys Compd 2019;777:524–30. https://doi.org/10.1016/j.jallcom.2018.10.376.
[10] Dai S, Bai Y, Shen W, Zhang S, Hu H, Fu J, et al. Core-shell structured Fe2O3@Fe3C@C nanochains and Ni–Co carbonate hydroxide hybridized microspheres for high-performance battery-type supercapacitor. J Power Sources 2021:482. https://doi.org/10.1016/j.jpowsour.2020.228915.

[11] Dai S, Zhang Z, Xu J, Shen W, Zhang Q, Yang X, et al. In situ Raman study of nickel bicarbonate for high-performance energy storage device. Nanomater Energy 2019;64:103919. https://doi.org/10.1016/j.nanoen.2019.103919.
[12] Young C, Park T, Yi JW, Kim J, Hossain MSA, Kaneti YV, et al. Advanced functional carbons and their hybrid nanoarchitectures towards supercapacitor applications. ChemSusChem 2018;11:3546–58. https://doi.org/10.1002/cssc.201801525.
[13] Wan L, Song P, Liu J, Chen D, Xiao R, Zhang Y, et al. Facile synthesis of nitrogen self-doped hierarchical porous carbon derived from pine pollen via MgCO3 activation for high-performance supercapacitors. J Power Sources 2019;438:227013. https://doi.org/10.1016/j.jpowsour.2019.227013.
[14] Jiang X, Guo F, Jia X, Zhan Y, Zhou H, Qian L. Synthesis of nitrogen-doped hierarchical porous carbons from peanut shell as a promising electrode material for high-performance supercapacitors. J Energy Storage 2020;30:101451. https://doi.org/10.1016/j.est.2020.101451.
[15] Gao Z, Zhang Y, Song N, Li X. Biomass-derived renewable carbon materials for electrochemical energy storage. Mater Res Lett 2017;5:69–88. https://doi.org/10.1080/21663831.2016.1250834.
[16] Li Y, Wang X, Cao M. Three-dimensional porous carbon frameworks derived from mangosteen peel waste as promising materials for CO2 capture and supercapacitors. J CO2 Util 2018;27:204–16. https://doi.org/10.1016/j.jcou.2018.07.019.
[17] Wei H, Wang H, Li A, Li H, Cui D, Dong M, et al. Advanced porous hierarchical activated carbon derived from agricultural wastes toward high performance supercapacitors. J Alloys Compd 2020;820:153111. https://doi.org/10.1016/j.jallcom.2019.153111.
[18] Sun K, Yu S, Hu Z, Li Z, Lei G, Xiao Q, et al. Oxygen-containing hierarchically porous carbon materials derived from wild jujube pit for high-performance supercapacitor. Electrochim Acta 2017;231:417–28. https://doi.org/10.1016/j.electacta.2017.02.078.
[19] Zhang J, Chen H, Bai J, Xu M, Luo C, Yang L, et al. N-doped hierarchically porous carbon derived from grape marcs for high-performance supercapacitors. J Alloys Compd 2021;854:157207. https://doi.org/10.1016/j.jallcom.2020.157207.
[20] Selvaraj AR, Muthusamy A, In-ho-Cho, Kim HJ, Senthil K, Prabakar K. Ultrahigh surface area biomass derived 3D hierarchical porous carbon nanosheet electrodes for high energy density supercapacitors. Carbon N Y 2021;174:463–74. https://doi.org/10.1016/j.carbon.2020.12.052.
[21] Zhang Y, Yu S, Lou G, Shen Y, Chen H, Shen Z, et al. Review of macroporous materials as electrochemical supercapacitor electrodes. J Mater Sci 2017;52:11201–28. https://doi.org/10.1007/s10853-017-0955-3.
[22] Liu S, Li A, Han Q, Yang C, Li H, Xia H, et al. Oxygen-directed porous activation of carbon nanospheres for enhanced capacitive energy storage. J Power Sources 2021;483:229223. https://doi.org/10.1016/j.jpowsour.2020.229223.
[23] Wang T, Xu Y, Shi B, Gao S, Meng G, Huang K. Novel activated N-doped hollow microporous carbon nanospheres from pyrrole-based hyper-crosslinking polystyrene for supercapacitors. React Funct Polym 2019;143:104326. https://doi.org/10.1016/j.reactfunctpolym.2019.104326.
[24] Zheng L, Dai X, Ouyang Y, Chen Y, Wang X. nHighly N/O co-doped carbon nanospheres for symmetric supercapacitors application with high specific energy. J Energy Storage 2021;33:102152. https://doi.org/10.1016/j.est.2020.102152.
[25] Zhou P, Wan J, Wang X, Xu K, Gong Y, Chen L. Nickel and cobalt metal-organic-frameworks-derived hollow microspheres porous carbon assembled from nanorods and nanospheres for outstanding supercapacitors. J Colloid Interface Sci 2020;575:96–107. https://doi.org/10.1016/j.jcis.2020.04.083.
[26] He D, Gao Y, Wang Z, Yao Y, Wu L, Zhang J, et al. One-step green fabrication of hierarchically porous hollow carbon nanospheres (HCNSs) from raw biomass: formation mechanisms and supercapacitor applications. J Colloid Interface Sci 2021;581:238–50. https://doi.org/10.1016/j.jcis.2020.07.118.
[27] Yaya A, Agyei-Tuffour B, Dodoo-Arhin D, Nyankson E, Annan E, Konadu DS, et al. Layered nanomaterials- A review. Glob J Eng Des Technol 2012;1:32–41.
[28] Apriwandi A, Taer E, Farma R, Setiadi RN, Amiruddin E. A facile approach of micro-mesopores structure binder-free coin/monolith solid design activated carbon for electrode supercapacitor. J Energy Storage 2021;40:102823. https://doi.org/10.1016/j.est.2021.102823.
[29] Liangshuo L, Lin Q, Xinyu L, Ming D, Xin F. Preparation of biomass-based porous carbon derived from waste ginger slices and its electrochemical performance. Optoelectron Adv Mater Rapid Commun 2020;14:548–55.
[30] Gou H, He J, Zhao G, Zhang L, Yang C, Rao H. Porous nitrogen-doped carbon networks derived from orange peel for high-performance supercapacitors. Ionics (Kiel) 2019;25:4371–80. https://doi.org/10.1007/s11581-019-02992-9.
[31] Brebu M, Vasile C. Thermal degradation of lignin – a review. Cellul Chem Technol Cellul Chem Technol 2009;44:353–63.
[32] Zhang Q, Han K, Li S, Li M, Li J, Ren K. Synthesis of garlic skin-derived 3D hierarchical porous carbon for high-performance supercapacitors. Nanoscale 2018;10:2427–37. https://doi.org/10.1039/c7nr07158b.
[33] Taer E, Handayani R, Apriwandi A, Taslim R, Awitdrus, Amri A, et al. The synthesis of bridging carbon particles with carbon nanotubes from areca catechu husk waste as supercapacitor electrodes. Int J Electrochem Sci 2019;14:9436–48. https://doi.org/10.20964/2019.10.34.
[34] Erabee IK, Ahsan A, Zularisam AW, Idrus S, Daud NNN, Arunkumar T, et al. A new activated carbon prepared from sago palm bark through physiochemical activated process with zinc chloride. Eng J 2017;21:1–14. https://doi.org/10.4186/ej.2017.21.5.1.
[35] Taslim R, Taer E, Siska M, Suedi, Suwandana, Agustino, et al. Synthesis of high porous activated carbon nanofibers using the single-step pyrolysis of reeds waste and its applications in supercapacitor electrodes. Technol Reports Kansai Univ 2020;62:5629–41.
[36] Taer E, Apriwandi A, Taslim R, Malik U, Usman Z. Single step carbonization-activation of durian shells for producing activated carbon monolith electrodes. Int J Electrochem Sci 2019;14:1318–30. https://doi.org/10.20964/2019.02.67.
[37] Girgis BS, Temerk YM, Gadelrab MM, Abdullah ID. X-ray diffraction patterns of activated carbons prepared under various conditions. Carbon Sci 2007;8:95–100. https://doi.org/10.5714/cl.2007.8.2.095.
[38] Wang Y, Qiao M, Mamat X. Nitrogen-doped macro-meso-micro hierarchical ordered porous carbon derived from ZIF-8 for boosting supercapacitor performance. Appl Surf Sci 2021;540:148352. https://doi.org/10.1016/j.apsusc.2020.148352.
[39] Taer E, Apriwandi, Dalimunthe BKL, Taslim R. A rod-like mesoporous carbon derived from agro-industrial cassava petiole waste for supercapacitor application. J Chem Technol Biotechnol 2021;96. https://doi.org/10.1002/jctb.6579.
[40] Kumar K, Saxena RK, Kothari R, Suri DK, Kaushik NK, Bohra JN. Correlation between adsorption and x-ray diffraction studies on viscose rayon based activated carbon

cloth. Carbon N Y 1997;35:1842–4. https://doi.org/10.1016/S0008-6223(97)87258-2.

[41] Deraman M, Daik R, Soltaninejad S, Nor NSM, Awitdrus A, Farma R, et al. A new empirical equation for estimating specific surface area of supercapacitor carbon electrode from X-ray diffraction. Adv Mater Res 2015;1108:1–7. https://doi.org/10.4028/www.scientific.net/AMR.1108.1.

[42] Roy CK, Shah SS, Reaz AH, Sultana S, Chowdhury AN, Firoz SH, et al. Preparation of hierarchical porous activated carbon from banana leaves for high-performance supercapacitor: effect of type of electrolytes on performance. Chem Asian J 2021;16:296–308. https://doi.org/10.1002/asia.202001342.

[43] Kuzmenko V, Naboka O, Haque M, Staaf H, Göransson G, Gatenholm P, et al. Sustainable carbon nanofibers/nanotubes composites from cellulose as electrodes for supercapacitors. Energy 2015;90:1490–6. https://doi.org/10.1016/j.energy.2015.06.102.

[44] Hor AA, Hashmi SA. Optimization of hierarchical porous carbon derived from a biomass pollen-cone as high-performance electrodes for supercapacitors. Electrochim Acta 2020;356:136826. https://doi.org/10.1016/j.electacta.2020.136826.

[45] Boyjoo Y, Cheng Y, Zhong H, Tian H, Pan J, Pareek VK, et al. From waste Coca Cola® to activated carbons with impressive capabilities for CO2 adsorption and supercapacitors. Carbon N Y 2017;116:490–9. https://doi.org/10.1016/j.carbon.2017.02.030.

[46] Azwar E, Wan Mahari WA, Chuah JH, Vo DVN, Ma NL, Lam WH, et al. Transformation of biomass into carbon nanofiber for supercapacitor application-A review. Int J Hydrogen Energy 2018;43:20811–21. https://doi.org/10.1016/j.ijhydene.2018.09.111.

[47] Chinnadurai D, Kim HJ, Karupannan S, Prabakar K. Multiscale honeycomb-structured activated carbon obtained from nitrogen-containing Mandarin peel: high-performance supercapacitors with significant cycling stability. New J Chem 2019;43:3486–92. https://doi.org/10.1039/C8NJ05895D.

[48] Duan B, Gao X, Yao X, Fang Y, Huang L, Zhou J, et al. Unique elastic N-doped carbon nanofibrous microspheres with hierarchical porosity derived from renewable chitin for high rate supercapacitors. Nanomater Energy 2016;27:482–91. https://doi.org/10.1016/j.nanoen.2016.07.034.

[49] Taer E, Apriwandi A, Taslim R, Agutino A, Yusra DA. Conversion Syzygium oleana leaves biomass waste to porous activated carbon nanosheet for boosting supercapacitor performances. J Mater Res Technol 2020;9:13332–40. https://doi.org/10.1016/j.jmrt.2020.09.049.

[50] Chen Y, Jiang Y, Liu Z, Yang L, Du Q, Zhuo K. Hierarchical porous N-doped graphene aerogel with good wettability for high-performance ionic liquid-based supercapacitors. Electrochim Acta 2021:366. https://doi.org/10.1016/j.electacta.2020.137414.

[51] Contescu CI, Adhikari SP, Gallego NC, Evans ND. Activated carbons derived from high-temperature pyrolysis of lignocellulosic Biomass. J Carbon Res 2018;4:9–13. https://doi.org/10.3390/c4030051.

[52] Yang V, Senthil RA, Pan J, Khan A, Osman S, Wang L, et al. Highly ordered hierarchical porous carbon derived from biomass waste mangosteen peel as superior cathode material for high performance supercapacitor. J Electroanal Chem 2019:113616. https://doi.org/10.1016/j.jelechem.2019.113616.

[53] Ghosh S, Barg S, Jeong SM, Ostrikov K. Heteroatom-Doped and oxygen-functionalized nanocarbons for high-performance supercapacitors. Adv Energy Mater 2020;10:1–44. https://doi.org/10.1002/aenm.202001239.

[54] Wang T, He X, Gong W, Sun K, Lu W, Yao Y, et al. Flexible carbon nano fibers for high-performance free-standing supercapacitor electrodes derived from Powder River Basin coal. Fuel 2020;278:117985. https://doi.org/10.1016/j.fuel.2020.117985.

[55] Fu Y, Zhang N, Shen Y, Ge X, Chen M. Micro-mesoporous carbons from original and pelletized rice husk via one- step catalytic pyrolysis. Bioresour Technol 2018;269:67–73. https://doi.org/10.1016/j.biortech.2018.08.083.

[56] Kumar TR, Senthil RA, Pan Z, Pan J, Sun Y. A tubular-like porous carbon derived from waste American poplar fruit as advanced electrode material for high-performance supercapacitor. J Energy Storage 2020;32:101903. https://doi.org/10.1016/j.est.2020.101903.